Maximizing Vanadium Redox Flow Battery Efficiency: Strategies of Flow Rate Control

Andrea Trovò
Department of Industrial Engineering
University of Padua
Padua, Italy
andrea.trovo@unipd.it

Francesco Picano
Department of Industrial Engineering
University of Padua
Padua, Italy
francesco.picano@unipd.it

Massimo Guarnieri
Department of Industrial Engineering
University of Padua
Padua, Italy
massimo.guarnieri@unipd.it

Abstract— **Vanadium redox flow batteries (VRFBs) are one of the most promising technologies for large-scale energy storage due to their flexible energy and power capacity configurations. The energy losses evaluation assumes a very important rule on the VRFB characterization in order increase the efficiency of the battery. Very few papers describe the relations between hydraulic, electrical and chemical contributions to the system energy losses, especially in a large size VRFB system. In the first part a fluid dynamics characterization of a 9kW / 27 kWh VRFB test facility has been conducted. In particular, we will consider the internal resistance as the sum of an ohmic and a transport resistance. Secondly, an overall loss assessment based on both numerical and experimental results has been carried out. Finally, some improvements in the battery management strategy and in stack engineering are proposed, that results from this work and can help the future designer to develop more efficient VRFB stack with a compact design.**

Keywords—Vanadium Redox Flow Battery, VRFB, flow rate management, shunt current, crossover, stack engineering.

I. INTRODUCTION

Energy storage technologies are playing a crucial role for a vast number of power electronic applications, such as renewable energy sources [1-3] electric vehicles [4-5], transport [6-7] and micro grids [8-10]. Several methods of energy storage have been recently studied and proposed in order to address these issues, including flywheel [11], supercapacitors and electrochemical storage (ESS) in large batteries [12]. Among the ESS technologies the redox flow batteries and especially the all vanadium Redox Flow Batteries (VRFBs) are emerging as a competitive option for stationary electrochemical energy storage, due to their intrinsic combination of advantages including power/energy decoupling, long cycle life, low environmental impact and operational flexibility [13-14]. VRFBs can successfully provide different services in future smart grids, e.g. peak shaving, load levelling, emergency backup [15], energy buffer for electric vehicle recharging stations and uninterruptible power supplies (UPS). These pros qualify VRFBs to play a significant role in the future energetic scenario. A large amount of work has been carried out in many laboratories in the last years, focused on the development of advanced materials with better performance

for electrolytes [16], membranes [17], and electrodes [18]. Several technological aspects have also been studied [19], but very few papers have been published on industrial-scale systems studied at a laboratory level for developing competitive technologies [20]. To this aim, the evaluation of losses in large VRFBs consisting of a stack made with many cells plays a pivotal role. Since VRFBs are based on two conductive liquid electrolytes flowing through couples of porous electrodes with ion-exchange membranes as separators, they are affected by three specific losses: hydraulic, electrical and chemical. The first type is strictly related to the friction losses in the porous electrodes and in the external piping. Electrical losses have two major origins [21]: a) During charge/discharge, the current flowing in the stack generate internal losses, mainly due to the resistive behavior of the ion-exchange membrane; b) The voltage gradient along the stack cells produces conduction currents (dubbed "shunt currents") in the solutions inside the stack piping resulting in Joule losses; c) Parasitic vanadium migration through the membrane due to its permeability (dubbed "species crossover") also result in energy losses [22]. Hydraulic losses depend on the flow rate management of the battery which in turn is related to the charge/discharge strategy adopted to provide energy storage, e.g. to the connected renewable sources, [23]. Several authors studied optimal strategies of electrolyte transport control, e.g. [24-25], but they generally missed to provide experimental data quantify the effect of flow rate control on the battery electric
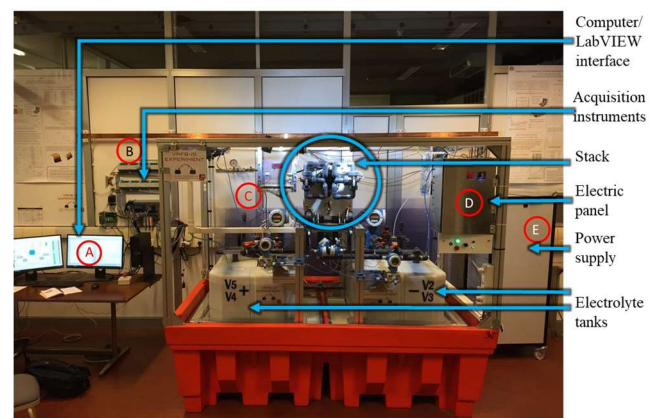

Fig.1 Energy storage Lab test facility

performance and cell internal losses modulation on the performance of a high power VRFB test systems.

This paper gives a contribution in this respect, with an experimental investigation on a VRFB test facility, installed at the Electrochemical Energy Storage and Conversion laboratory of the University of Padua (Fig. 1). The paper also presents the evaluation of the other loss contributions, i.e. chemical and electrical, in the IS-VRFB test facility. Simulations from numerical model are validated against experimental data. The information provided can address the design of control systems of next-generation high-performance VRFBs.

II. EXPERIMENTAL SET-UP

IS-VRFB is provided with a compact stack of $N = 40$ cells with 600 cm^2 active area capable of operating at 9 kW [26-27]. As usual cell inside the stack are electrically connected in series and hydraulically fed in parallel. Two 550-liter polyethylene tanks contain the positive and negative 1.6 M vanadium solutions in 4.5 M sulfuric acid which allow to store 27 kWh. Each cell consists of two thick carbon-felt electrodes separated by a Nafion® 212 membrane, placed between two sintered graphite bipolar plates. This structure is enclosed in polyethylene frames provided with thin branched channel for distributing the solutions in the porous electrodes from the large manifolds at the cell corners. Solutions are circulated between tanks and stack in PVC piping provided with centrifugal pumps powered by inverter-driven induction motors, which allow a maximum flow rate of 29.5 L min^{-1}. The system is fully instrumented with thermo-fluid dynamic and electrical probes. Each inverter is controlled by a voltage analog input. The energy for charging or discharging the battery is controlled by an electronic two-quadrant power supply. The data acquisition and control system is built on a National Instruments compact DAQ interface connected to a computer. In-house LabVIEW routines allow processing all experiment measurements and controlling experiment parameters (flow rates and stack current) on proper feedback bases Fig.1.

III. VRFB MODELLIZATION

A cell-resolved dynamic model was developed for simulating the different terms of the energy losses of the IS-VRFB: hydraulic pressure drops, crossover inherent side reactions, and shunt current. The model is based on energy and mass balance equations coupled with an equivalent electric circuit for computing shunt currents.

A. Hydraulic model

The total pump hydraulic power demand P_h results from the stack P_s and the piping P_{pi} contributions:

$$P_h = P_s + P_{pi}$$
$$P_s = Q_+ \Delta p_{s+} + Q_- \Delta p_{s-} \qquad (1)$$
$$P_{pi} = Q_+ \Delta p_{pi+} + Q_- \Delta p_{pi-}$$

The stack pressure drop Δp_s at different flow rates Q in the positive and negative circuits were obtained from direct

measurements on the IS-VRFB, whereas the piping pressure drop Δp_{pi} as a function of the flow rate Q in each circuit was computed by using an experimentally validated numerical model that uses standard equations [28], complemented with figures from the components data sheets. The total hydraulic piping and stack losses in a whole cycle were obtained by integrating P_s and P_{pi} during charge and discharge, by means of LabVIEW routines.

B. Electrical model

Shunt currents arise in the hydraulic circuit inside the stack because the conductive solutions are fed in parallel, through manifolds and distribution channels, to homologous cell electrodes which are at different electrical potentials, Fig.2. These currents were computed by means of an equivalent electrical circuit exemplified in Fig. 2. Each cell was represented as a Thévenin equivalent made of an ideal voltage generator E_0 in series with a resistance R_i, both parameters being dependent on the battery state of charge (SOC, later on indicated as s) and the latter also on the solution flow rates Q [29]. R_i result from the resistances which takes into account the cell overpotentials: activation R_a, ohmic (membrane) R_o, and transport R_t [30]:

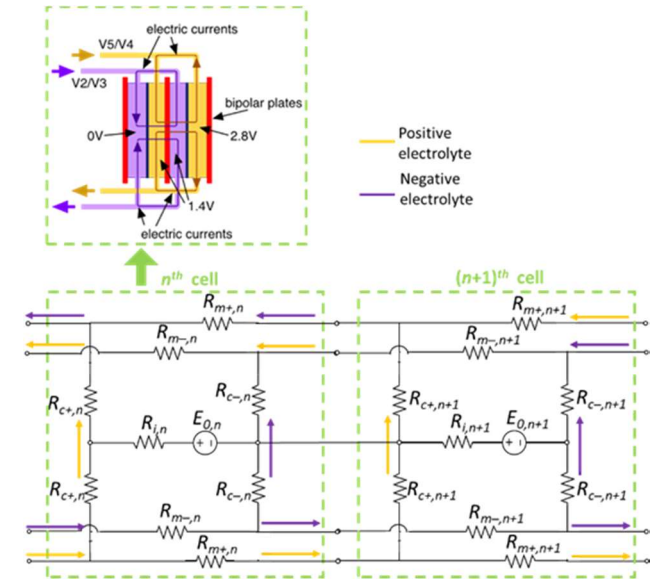$$R_i = R_a + R_o + R_t \qquad (2)$$

Fig.2 IS-VRFB stack equivalent electric model

The circuit segments inside the stack, i.e. cell's manifold segments, flow channels and felts, were modeled as resistors. The electric resistances of the tubular segments of manifolds and flow channels were computed as:

$$R_{k\pm} = l_k / [\sigma_\pm(s) A_k] \qquad (3)$$

where l = segment length, A = segment cross section, $k = m$ (manifolds) and $k = c$ (flow channels), and +,– stand for the positive and negative electrolytes. The electrolyte conductivity σ depends on the vanadium species
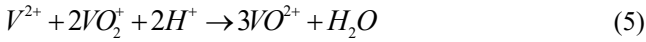
concentrations, hence on the *SOC* s [31]. The contributions of the porous felts to R_c were computed after a numerical fluid-dynamic analysis. Shunt-current losses P_{sc} in all circuit segments were computed from the currents i and voltages v in each circuit element, whereas the total cell internal power losses were calculated as:

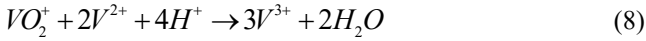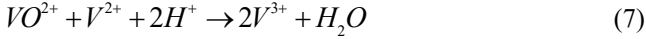$$P_i = \sum\nolimits_{cell} R_i i^2 \qquad (4)$$

The shunt current energy losses W_{sc} and cell internal energy losses W_i along a whole operation cycle were obtained by integrating P_{sc} and P_i during charge and discharge. The complete description of the stack electric model is reported in [29] and [31].

C. Crossover model

The cell membrane has the functions to separate the positive and the negative compartments while allowing hydrogen ions passing. Indeed, some permeation occurs resulting in species crossover, that is followed by exothermic side reactions without electric energy conversion, resulting in self-discharge of the solution in the stack. In particular, the species V^{3+} and V^{2+} which arrive at the positive compartment from the negative one react with VO_2^+ as [32]:

$$V^{2+} + 2VO_2^+ + 2H^+ \rightarrow 3VO^{2+} + H_2O \qquad (5)$$

$$V^{3+} + VO_2^+ \rightarrow 2VO^{2+} \qquad (6)$$

and the species VO^{2+} and VO_2^+ which arrive at the negative compartment from the positive one react with V^{2+} as [32]:

$$VO^{2+} + V^{2+} + 2H^+ \rightarrow 2V^{3+} + H_2O \qquad (7)$$

$$VO_2^+ + 2V^{2+} + 4H^+ \rightarrow 3V^{3+} + 2H_2O \qquad (8)$$

The reactions (5–8) were taken into account in the mass balance equations, together with the Fick's laws modeling the vanadium ions crossover. The resulting crossover model, that is described in detail in [31], allows calculating the crossover (i.e. chemical) power losses P_{co} of the VRFB.

D. Power losses characterization

Several efficiency definitions are used in the literature to quantify the performance of a VRFB, e.g. coulombic efficiency, voltage efficiency, energy efficiency [24]. For the purpose of this work the more inclusive definition consists of the round-trip energy efficiency (*RTE*), that take into account all the aforementioned losses occurring in a VRFB system during charge (*ch*) and discharge (*dc*):

$$RTE = \frac{\int_0^{t_{dc}} P - P_w \, dt}{\int_0^{t_{ch}} P + P_w \, dt} \qquad (9)$$

P is the electrical power at the stack terminals and P_w is the total hydraulic power supplied from the grid to the pump inverters, which was measured with a wattmeter (Fig. 3). The power was delivered by the inverters with an efficiency $\eta_{in} =$

0.95 (data sheet figure), by the induction motor with efficiency $\eta_{mo} = 0.5$ (after bench tests on a similar electric motors), and by the pump with an efficiency η_{pu}, which was determined by means of tests made on the plant. Finally, the pumps provide the overall hydraulic power losses P_h described in eq. (1).
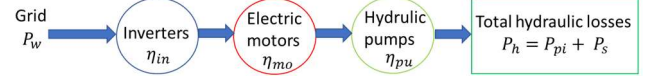

Fig.3 Flow of power of the ancillary devices.

As regards *RTE*, a Sankey diagram provides a quick representation of how *RTE* is built up from the grid P_s due to the of the different loss terms. Fig.4 represents their effects on the power P taken from the grid and provided to the stack in relation with the power P_{st} that is converted into stored energy during a charge operation. Similar considerations hold in the discharge phase.
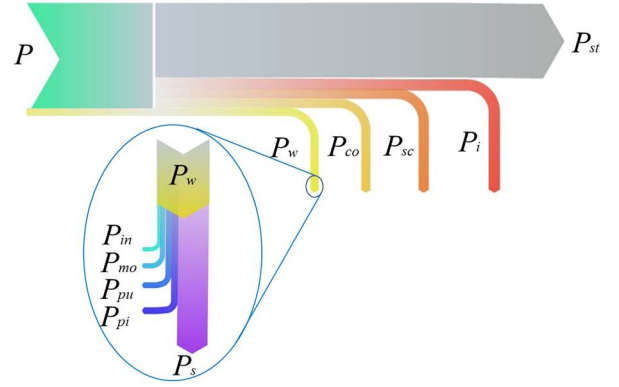

Fig.4 Sankey diagram of the power flows during charge. P= power delivered to the stack, P_{st} power converted in stored energy in the battery electrolytes.

IV. RESULTS AND DISCUSSIONS

A. Experimental results on flow rate optimization

The first part of this work aims at investigating actions to achieve improvements in the Q-related losses of a VRFB, namely higher-*RTE* control algorithm to be implemented in the battery management system and also better cell and stack designs. The instigation is centered on identifying the optimal Q, in order to preserve high electric performance while avoiding unnecessary losses, particularly reducing the internal resistance R_i as much as possible. The analysis made use of the electrolyte flow factor α, that indicates the ratio between the electrical charges in the flowing electrolyte and the electric current:

$$\alpha = \begin{cases} QFCs/Ni & \text{discharge} \\ QFC(1-s)/Ni & \text{charge} \end{cases} \qquad (10)$$

where $F = 96485$ C mol^{-1} is the Faraday constant and C is the total vanadium molar concentration in the electrolyte. A

unitary flow factor $\alpha = 1$ is the minimum possible value in which all flowing charge porters react at the electrode, to provide the stack electric current. $\alpha = 1$ would be the ideal working conditions as regards minimizing the pumping power. Unfortunately, it is dangerous, to use such a small α value, because not all charge porters are able reach the active sites and actually react while flowing in the porous electrodes, resulting in cell failures and damages [21]. In practical cases, α is usually kept at higher values, usually between seven and eight. Fig. 5 shows some polarization curves during discharge at different α for *SOC*s between 20% and 60%. Similar curves were obtained in charge. The marked linearity of these curves at fixed α highlight a constant internal resistance R_i and reveals that activation losses (i.e. R_a), which should cause non-linearity at low current, are negligible. When the flow factor exceeds a critical saturation value α_{sat}, the polarization curves tend on a single profile with minimum slope, i.e. minimum resistance.
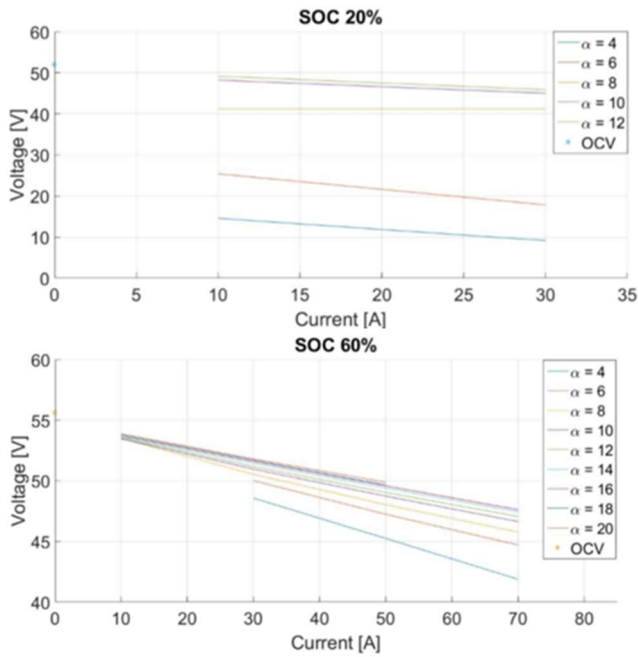

Fig.5 Polarization curve at different *SOC*s and flow factor during discharge.

This behavior reveals that the electrical performance cannot be enhanced by increasing further Q. It also highlights that when the VRFB is operated at fixed Q, as long as α is higher than a saturation value α_{sat}, its cell behavior is dominated by the ohmic resistance R_o and the slope of $v(i)$ is minimal. Conversely, transport losses, accounted for by R_t, are not negligible when $\alpha < \alpha_{sat}$. The Ohmic resistance only depends mostly on the ion exchange membrane and can't be minimized by means Q management strategies. These results suggest further investigations to identify an optimal α that is *SOC* and current dependent, capable of minimizing the overall power losses in each condition, so as to maximize the battery *RTE*. As discussed above, the electrolyte flow rate affects the internal stack resistance according to the transport resistance R_t that contributes to R_i: the higher Q, the lower R_t, R_i and P_i. On the other hand, Q also affects the hydraulic

losses P_h both in the stack and in the piping terms. Conversely, crossover chemical losses P_{co} and shunt current losses P_{sc} are not directly affected by Q, as shown above. Consequently, the losses which mainly depend on Q are P_i and P_h:

$$P_t(Q) = P_i + P_h \tag{11}$$

Minimizing eq. (11) provides the optimal Q value in each operating condition. By analyzing the experimental data, an optimal flow rate strategy as a function of different *SOC*s and stack currents i was identified. The battery losses as functions of Q were analyzed at different *SOC*s in the range from 20% to 80%, with battery currents controlled at 10, 30, 50, and 70 A.
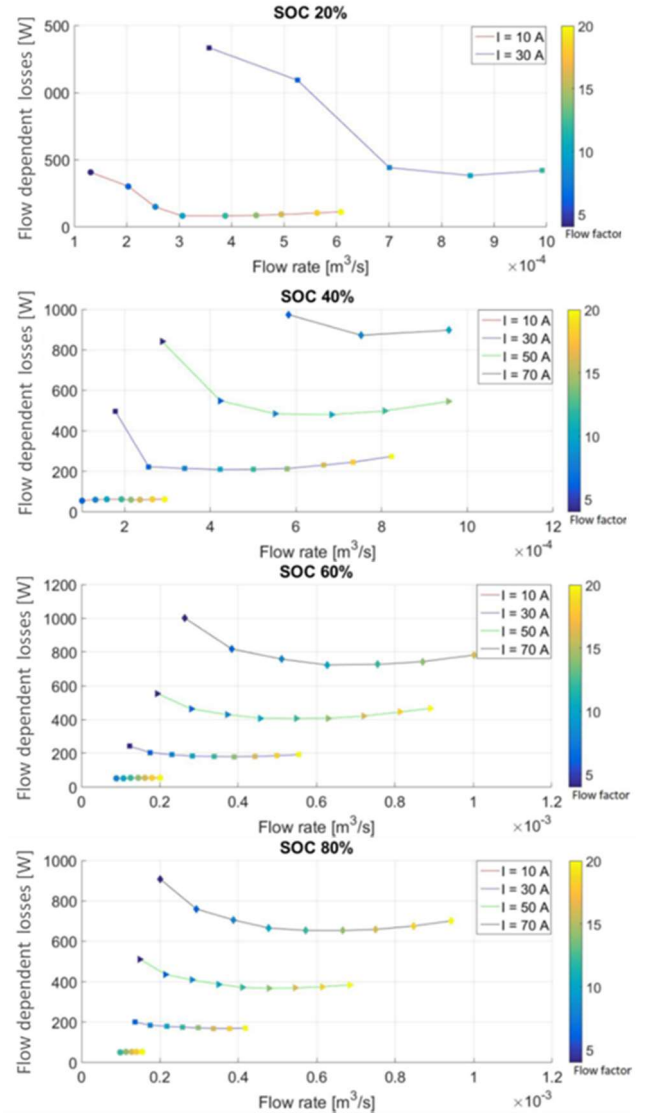

Fig.6 Flow rate dependent losses at different SOCs, current and flow factor during discharge.

The explored Q depended on the capability of the device hydraulic system. Q below 2 L min^{-1} cause cell voltage below 0.1 V, which can damage the porous electrodes while Q above 29.5 L min^{-1} are prevented by the pumps rating. Thus, the

study was carried out for Q in such range (Fig. 6). From Fig. 6 the optimal flow rate and consequently the optimal flow factor, which gives the lowest flow dependent losses, can be deduced. In such optimal conditions, the RTE is maximized. Those results can address the development of an advanced high-RTE flow rate management system.

B. Battery losses evaluation

Tab. 1. Numerical and experimental energy terms and system efficiencies during charge/discharge cycles.

I	SOC range	W_{ch} (exp)	W_{dc} (exp)	W_w (exp)	W_i (num)	W_{sc} (num)	W_{co} (num)	RTE (exp)	RTE (num)	Rel. error.
A	%	[Wh]	[Wh]	[Wh]	[Wh]	[Wh]	[Wh]	%	%	%
30	13.1 − 87	17941	13610	1205	1991	2049	2771	70.35	70.72	+0.53
50	19.9 − 78.5	14273	10165	717	2473	985	1340	67.10	66.67	−0.64
70	28.0 − 78.7	10809	7133	492	2406	515	699	62.42	62.81	+0.62

In this session all types of losses are evaluated in detail, both numerically and experimentally under some operating conditions. These studies, making use of both measurements and simulations, were performed at three current values of 30 A, 50 A and 70 A. In all cases, a constant $\alpha = 8$ was used during each charge/discharge cycle. This α figure is close to the value of 7.5 which was claimed as optimal in a study conducted on a 40-cell stack [24]. Firstly, a model validation was carried out by comparing experimental and numerical RTE values (Tab.1). Numerical simulations considered the same external conditions that occurred during the experimental charge and discharge cycles. W_{ch}, W_{dc} and W_w in the third, fourth and fifth columns of Tab.1 were obtained by integration of measurements, performed with Labview routines. W_i, W_{sc} and W_{co} were computed within the model. The good agreement between the experimental and numerical values of the RTE is attested by relative errors below 1% and, together with a further experimental validation of the model presented in [31], [33] confirms the model reliability. The bar diagrams in Fig. 7 represent the graphical representation of the computed losses in Tab.1. The ancillary energy losses W_w needed for circulating the solutions assume a higher relative importance in the case of low-current charge/discharge cycles, due to the longer duration of the operation. In the 30 A case, $W_w = 1205$ W h was measured, more than twice that at 70 A. In addition, the hydraulic losses in the stack and piping correspond together only at about 10% of W_w. This is due to the low efficiencies of the devices (motors and impellers) used in the solution circulating system, as reported in the previous section but also underlines the relative low impact of the hydraulic losses in comparison to the other loss terms. A decreasing dependence with the stack current is shown in the other loss terms, i.e. crossover and shunt current losses, because of the longer operation time. Conversely, an increase of the cell internal losses P_i with the stack current was found, that calls for cell engineering improvements focused on reducing the internal loses (i.e. R_i), in order to increase the battery efficiency at high current operation. It must also be noted, that shunt current losses have not a marginal effect on the total amount of losses and consequently on the VRFB efficiency.
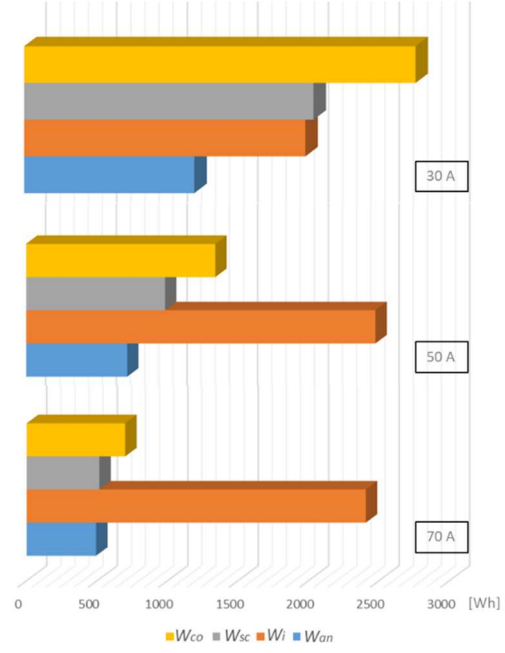

Fig.7. Battery energy losses contributions at different stack currents at $\alpha = 8$.

V. CONCLUSIONS

The present study has been based on IS-VRFB, an industrial-scale test facility, and is addressed in identifying improvements in the battery management as regard the flow rate management strategy as well as in the stack design of a next compact VRFB systems. The effect of the flow rate and of the flow factor on the electric performance during the discharge phase have been investigated, finding that two technological drivelines can be followed to improve the power performances of a VRFB stack. On the one hand, it is crucial to control the flow rate, avoiding flow factors above the saturation value α_{sat}. Actions for reducing it as much as possible are advisable, e.g. by means of more efficient porous electrodes to enhance the porous dispersion on the active sites through an innovative design, while keep drag as low as possible. On the other hand, a decrease of the ohmic resistance R_o can reduce the losses at high stack current, as shown in the analysis described in Section IV-B, regarding the internal cell losses W_i along an entire cycle. To this aim, the investigations should be focused on the cell engineering, namely on reducing the electrode thickness, increasing its compression and/or reducing the electric resistance of the conductive materials and, particularly, the contact resistances inside the cell. Moreover, this study provides an original method, developed on an extensive experimental campaign that aims at optimizing the flow rate in order to minimize the flow-rate dependent losses (Fig.6). In agreement with these results, an advanced flow management strategy based on the optimal flow factor profiles in each operating condition has been implemented by using LabVIEW routines. It was found an increment of around 2% in comparison to the RTE values of Tab.1, where a constant $\alpha = 8$ was used, that are considered as an optimal value in previous literature [24]. The loss analyses highlighted the relative low impact of the hydraulic losses in the stack and external piping, considering that they

account about for 10% of the whole ancillary (i.e. solution circulating system) energy losses. This result suggests to select high-efficiency devices. It also indicates that compact VRFB stacks with a quite high number of cells should be designed with a special care to reduce shunt currents, with marginal consequences on the hydraulic performance: thinner and longer flow paths should be preferred in the trade-off between shunt current and hydraulic losses minimization.

REFERENCES

[1] S.J. Chiang, K.T. Chang and C.Y. Yen. Residential Photovoltaic Energy Storage System. IEEE Ind Electron vol. 45, no. 3, pp. 385-394; 1998.

[2] Y. Yang, Q. Ye, L.J. Tung, M. Greenleaf and H. Li. Integrated Size and Energy Management Design of Battery Storage to Enhance Grid Integration of Large-Scale PV Power Plants. IEEE Ind Electron. vol. 65, no. 1, pp. 394-402, 2018.

[3] S.T. Kim, S. Bae, Y.C. Kang and J.W. Park. Energy Management Based on the Photovoltaic HPCS With an Energy Storage Device. IEEE Ind Electron. vol. 62, no. 7, pp. 4608—4617, 2015.

[4] W. Huang and J.A.A. Qahouq. Energy Sharing Control Scheme for State-of-Charge Balancing of Distributed Battery Energy Storage System. IEEE Ind Electron. vol. 62, no.5, pp. 2764-2776, 2015.

[5] N. Li, F. Gao, T. Hao, Z. Ma and C. Zhang. SOH Balancing Control Method for the MMC Battery Energy Storage System. IEEE Ind Electron. vol. 65, no. 8, pp. 6581-6591, 2018.

[6] S. Vazquez, S. M. Lukic, E. Galvan, L. G. Franquelo and J. M. Carrasco. Energy Storage Systems for Transport and Grid Applications. IEEE Ind Electron. vol. 57, no. 12, pp. 3881- 3895, 2010.

[7] I. Perin, G. R. Walker and G. Ledwich. Load Sharing and Wayside Battery Storage for Improving AC Railway Network Performance, With Generic Model for Capacity Estimation, Part 1. IEEE Ind Electron. Vol. 66, no. 3, pp. 1791- 1798, 2019.

[8] S. M P, M. Das, V. Agarwal. Design and Development of a Novel High Voltage Gain, High-Efficiency Bidirectional DC–DC Converter for Storage Interface. IEEE Ind Electron. vol, 66, no. 6, pp. 4490-4501, 2019.

[9] Y. Li, Z. Yang, G. Li, D. Zhao and W Tian. Optimal Scheduling of an Isolated Microgrid With Battery Storage Considering Load and Renewable Generation Uncertainties. IEEE Ind Electron. Vol. 66, no. 2, pp. 1565- 1575, 2019.

[10] F.G. Torres, C. Bordons and M.A. Ridao. Optimal Economic Schedule for a Network of Microgrids With Hybrid Energy Storage System Using Distributed Model Predictive Control. IEEE Ind Electron. vol. 66, no. 3, pp. 1919-1929, 2019.

[11] X. Li, B. Anvari, A. Palazzolo, Z. Wang, and Hamid Toliyat. A Utility-Scale Flywheel Energy Storage System with a Shaftless, Hubless, High-Strength Steel Rotor. IEEE Ind Electron. vol. 65, no. 8, pp. 6667-6675, 2018.

[12] L. Zhang, Y. Tang, S. Yang and F. Gao. Decoupled Power Control for a Modular- Multilevel-Converter-Based Hybrid AC–DC Grid Integrated with Hybrid Energy Storage. IEEE Ind Electron. vol. 66, no. 4, pp. 2926- 2934, 2019.

[13] P. Alotto, M. Guarnieri and F. Moro. Redox flow batteries for the storage of renewable energy: A review. Renew Sustain Energy Rev, vol. 29, pp. 325-335, 2014.

[14] M. Guarnieri, P. Mattavelli, G. Petrone and G. Spagnuolo. Vanadium redox flow batteries: Potentials and challenges of an emerging storage technology. IEEE Ind Electron Mag; vol. 10, no. 4, pp. 20-31, 2016.

[15] H. Al-Fetlawi, A.A. Shah and F. C. Walsh. Non-isothermal modelling of the all-vanadium redox flow battery. Electrochim Acta vol.55, pp. 78-79, 2009.

[16] S. Roe, C. Menictas and M.Skyllas-Kazacos. A High Energy Density Vanadium Redox Flow Battery with 3 M Vanadium Electrolyte. J Electrochem Soc; vol. 163, pp. A5023-A5028, 2016.

[17] C. Sun, A. Zlotorowicz, G. Nawn, E. Negro, F. Bertasi, G. Pagot, K. Vezzù, G. Pace, M. Guarnieri and V. Di Noto. [Nafion/(WO3)x] hybrid membranes for vanadium redox flow batteries. Solid State Ionics; vol. 319, pp. 110-116, 2018.

[18] D. Maggiolo, F. Zanini, F. Picano, A. Trovò, S. Carmignato and M. Guarnieri. Particle based method and X-ray computed tomography for pore-scale flow characterization in VRFB electrodes. Energy Storage Mater; vol. 16, pp. 91-96, 2019.

[19] F.T. Wandschneider, S. Röhm, P. Fischer, K. Pinkwart, J. Tübke and H. Nirschl. A multi-stack simulation of shunt currents in vanadium redox flow batteries. J Power Sources, vol. 261, pp. 64-74, 2014.

[20] L. F. Arenas, C. Ponce de León and F.C. Walsh. Engineering aspects of the design, construction and performance of modular redox flow batteries for energy storage. J Energy Storage; vol. 11, pp. 119-153, 2017.

[21] T. Wang, J. Fu, M. Zheng and Z. Yu. Dynamic control strategy for the electrolyte flow rate of vanadium redox flow batteries. Appl Energy; vol. 227, pp. 613–623, 2018.

[22] S. Won, K. Oh and H. Ju. Numerical analysis of vanadium crossover effects in all-vanadium redox flow batteries. Electrochim Acta; vol. 177, pp. 310-320, 2015.

[23] M. J. Watt-Smith, P. Ridley, R. G. A. Wills, A.A. Shah and F.C. Walsh. The importance of key operational variables and electrolyte monitoring to the performance of an all vanadium redox flow battery. J Chem Technol Biotechnol; vol. 88, pp. 126-138, 2013.

[24] A. Tang, J. Bao and M. Skyllas-Kazacos. Studies on pressure losses and flow rate optimization in vanadium redox flow battery. J Power Sources; vol. 248, pp. 154-162, 2014.

[25] J. Houser, A. Pezeshki, J. T. Clement, D. Aaron and M. M. Mench. Architecture for improved mass transport and system performance in redox flow batteries. J Power Sources; vol. 351, pp. 96-105, 2017.

[26] M. Guarnieri, A. Trovò, A. D'Anzi and P. Alotto. Developing vanadium redox flow technology on a 9-kW 26-kWh industrial scale test facility: Design review and early experiments. Appl Energy, vol. 230, pp. 1425-1434, 2018.

[27] M. Guarnieri, A. Trovò, G. Marini, A. Sutto and P. Alotto. High current polarization tests on a 9 kW vanadium redox flow battery. J Power Sources, vol. 431, pp. 239-249, 2019.

[28] B.R. Munson, T.H. Okiishi, W.W. Huebsch and A.P. Rothmayer. Fundamentals of fluid mechanic. New York, NY: John Wiley & Sons, 2012.

[29] F. Moro, A. Trovò, S. Bortolin, D. Del Col and M. Guarnieri. An alternative low-loss stack topology for vanadium redox flow battery: Comparative assessment. J Power Sources; vol. 340, pp. 229-241, 2017.

[30] L. J. Ontiveros and P. E. Mercado. Modeling of a Vanadium Redox Flow Battery for power system dynamic studies. Int J Hydrogen Energy; vol.39, pp. 8720-8727, 2014.

[31] A. Trovò, G. Marini, A. Sutto, P. Alotto, F. Moro, M. Giomo and M. Guarnieri. Standby thermal model of a vanadium redox flow battery stack with crossover and shunt-current effects. Appl Energy; vol. 240, pp. 893-906, 2019.

[32] A. Tang, J. Bao and M. Skyllas-Kazacos. Thermal modelling of battery configuration and self-discharge reactions in vanadium redox flow battery. J Power Sources; vol. 216, pp. 489–501, 2012.

[33] A. Trovò, A. Saccardo, M. Giomo and M. Guarnieri. Thermal modelling of industrial-scale vanadium redox flow batteries in high current operations. J Power Sources; vol. 424, pp. 204-214, 2019.